



# A Compact Model for Drift and Diffusion Memristor Applied in Neuron Circuits Design

Ying Zhao, Cong Fang, Xumeng Zhang<sup>ID</sup>, Xiaoxin Xu, Tiancheng Gong, Qing Luo<sup>ID</sup>, Chengying Chen, Qi Liu<sup>ID</sup>, Hangbing Lv<sup>ID</sup>, Qiang Li, *Senior Member, IEEE*, Feng Zhang<sup>ID</sup>, Ling Li, and Ming Liu<sup>ID</sup>, *Fellow, IEEE*

**Abstract**—A compact model of memristor for unifying two switch characteristics, drift and diffusion, has been proposed. The switching mechanism is based on the ion dynamic transport theory at the oxide interface layer. The model is verified by experimental data in different oxide material-based drift memristors and new emerging diffusion memristors. Under parameter variations and temperature evolution, this model well fits dc/ac characteristics of both devices. Moreover, the compact model is coded in Verilog-A and implemented in a vendor CAD environment. As case studies, the applications of this model in the neuromorphic circuit design to replace the traditional CMOS circuits are shown.

**Index Terms**—Compact model, memristor, neuromorphic circuits, Verilog-A.

## I. INTRODUCTION

RECENTLY, various types of memristors, such as ion drift (drift type) and diffusion (diffusion type), are promising to be a candidate for enabling high-density and ultimately

Manuscript received June 8, 2018; revised July 24, 2018; accepted August 6, 2018. This work was supported in part by the National Key Research Plan of China under Grant 2018YFB0407500, in part by the National Natural Science Foundation of China under Grant 61704143, Grant 61474134, and Grant 61720106013, and in part by the Young and Middle-Aged Teacher Education Research Project of Fujian Province under Grant JAT170428. The review of this paper was arranged by Editor G. Koh. (*Corresponding authors: Feng Zhang; Ling Li*)

Y. Zhao is with the Key Laboratory of Microelectronics Devices and Integrated Technology, Institute of Microelectronics of Chinese Academy of Sciences, Beijing 100029, China, and also with the Institute of Integrated Circuits and Systems, University of Electronic Science and Technology of China, Chengdu 610054, China (e-mail: zhaoying@ime.ac.cn).

C. Fang, X. Zhang, X. Xu, T. Gong, Q. Luo, Q. Liu, H. Lv, F. Zhang, L. Li, and M. Liu are with the Key Laboratory of Microelectronics Devices and Integrated Technology, Institute of Microelectronics of Chinese Academy of Sciences, Beijing 100029, China (e-mail: 15120004@bjtu.edu.cn; zhangxumeng@ime.ac.cn; xuxiaoxin@ime.ac.cn; gongtiancheng@ime.ac.cn; luqing@ime.ac.cn; liuqi@ime.ac.cn; lvhangbing@ime.ac.cn; zhengfeng\_ime@ime.ac.cn; lingli@ime.ac.cn; liuming@ime.ac.cn).

C. Chen is with the School of Microelectronics, Xiamen University of Technology, Xiamen 361005, China (e-mail: chenchengying363@163.com).

Q. Li is with the Institute of Integrated Circuits and Systems, University of Electronic Science and Technology of China, Chengdu 611731, China (e-mail: qli@uestc.edu.cn).

Color versions of one or more of the figures in this paper are available online at <http://ieeexplore.ieee.org>.

Digital Object Identifier 10.1109/TED.2018.2865225

scaled synaptic arrays in neuromorphic architectures [1]–[4]. The drift-type memristors as synaptic devices to emulate synaptic functions have recently been demonstrated [3], [4]. However, the characteristics of them [5] do not faithfully replicate the nature of synaptic plasticity [6]. A device with a similar physical behavior to the biological  $\text{Ca}^{2+}$  dynamics would enable improved simulation of the synaptic function and broad applications to neuromorphic computing [1]. The dynamic properties of diffusion-type memristors are functionally similar to  $\text{Ca}^{2+}$  in biological synapses. It is experimentally demonstrated that the diffusion type has a great performance of dynamic plasticity, such as pair-pulse facilitation and depression [1]. Furthermore, the compact model of the memristor is indispensable in the neuromorphic circuit design. So far, many types of research have been done for modeling the switching behavior of different metal–oxide-based memristors based on the subcircuits [7]–[18]. However, the physics-based compact model of the memristor operating available is still scarce for the neuromorphic circuit simulation. As far as we know, the compact model used for both emerging drift and diffusion memristors is still lacking.

In this paper, a physics-based compact model applicable for both drift and diffusion memristors is developed based on the insight of the ion transport theory under the effect from the Joule thermal effect, interface energy diffusion, and electric field. Furthermore, the proposed model is used in the classical neural circuit design with great accuracy of circuit performance estimation.

## II. DEVICE MODEL

### A. Device Physical Mechanism

The resistive switch mechanism here is subjected to the creation and breakdown of the conductive filament (CF) in the oxide layer [2], [5], [8], [19]. Drift and diffusion devices have different initial states, as shown in Figs. 1(a) and 2(a), but the SET processes of both drift and diffusion devices are attributed to the dielectric soft breakdown and the creation of CFs by a positive voltage on the top electrode (TE), as shown in Figs. 1(b) and (c) and 2(b) and (c). The generated vacancies/ions inside the oxide layers drift to TE and form CFs. After the SET process, the devices get to the low-resistance state (LRS) from the high-resistance state (HRS).

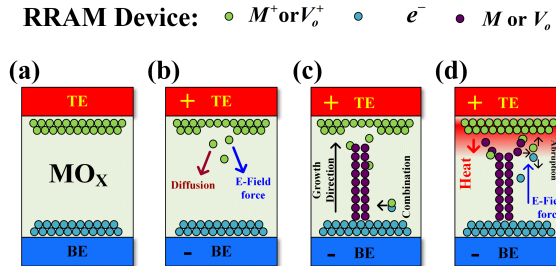


**Fig. 1.** Schematic physical processes of resistive switching for the drift memristor. (a) Initial state. (b) and (c) SET process: CF formed by applying the positive voltage on TE. (d) RESET process: the reverse voltage and Joule heat are dominant for CF rupture.

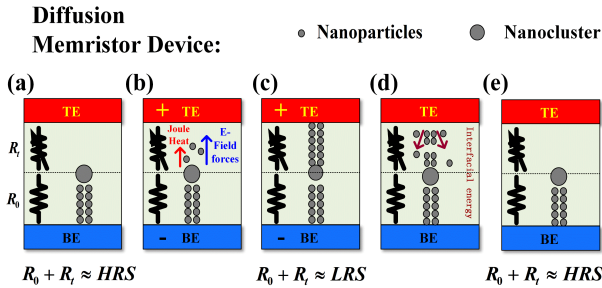


**Fig. 2.** Schematic physical processes of resistive switching for the diffusion memristor. (a) Initial state: the particles inside the device form clusters, the CFs between the cluster and BE are equivalent to an ohmic resistance  $R_0$ . (b) SET process: the CFs formed by applying a positive voltage. (c) CFs connects the electrodes making device in the LRS. (d) and (e) RESET process: after the removal of the voltage, the device returns to the HRS due to the interaction of the minimal potential energy of the interface.

Although the RESET process is attributed to the CF rupture, the mechanisms behind are different between the drift and diffusion devices. For the drift one, it is the recombination of vacancies and ions induced by the positive voltage applied on the bottom electrode (BE) or Joule heat [Fig. 1(d)]. The vacancies/ions are released and recombine with other vacancies/ions that have the opposite charge. The RESET process of drift devices will not happen unless there is a positive voltage applied on BE [5]. For the diffusion one, it is the particle diffusion toward the minimum energy positions near the device terminals [1]. After withdrawing the positive voltage from TE, the particles will be released by TE and diffuse to many small wells between the electrodes [Fig. 2(d)], due to the interfacial energy and the nanoparticle-pinning energy minimization [1], [20]. The diffusion-type devices will switch to HRS from LRS without the help of positive voltage on BE [Fig. 2(e)].

### B. Compact Model

Inspired by the original circuit model proposed by Hewlett-Packard for  $TiO_2/TaO_2$ -based devices [21], the equivalent circuit of the proposed compact model is depicted in Fig. 3. The total resistance  $R(x)$  of the memristors relevant to the state of internal particles is a sum of an ohmic resistance  $R_0$  and a tunneling variable resistance  $R_t$ .  $R_0$  represents the resistance of the existed filament region and  $R_t$  represents the tunneling resistance between the filament and the interface. This equivalent circuit is suitable for both drift and diffusion

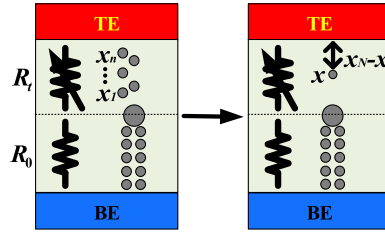


**Fig. 3.** Equivalent circuit of coupled ohmic-tunneling resistor circuit model.

models

$$R(x) = R_0 + R_t. \quad (1)$$

The key variable of this model is the derivative of  $x$  with respect to time ( $dx/dt$ ). After the characteristics of the two types of memristors are reproduced by adjusting ( $dx/dt$ ), the compact model for the circuit design can be made

$$\frac{dx}{dt} = f(V, T, x) \quad (2)$$

$$x = \int f(V, T, x) + \chi(i) dt \quad (3)$$

where  $x$  is defined as a gap (drift device) or position (diffusion device) between the top of CF and TE and  $\chi(i)$  is the Gaussian noise sequence. The model makes an assumption of particle normalization based on the thought of mean value, in which  $\mathbf{x} \cong \sum_{i=0}^n \mathbf{x}_i$ , as shown in Fig. 3. The positions of particles inside the devices are normalized to the position of one particle. The resistance variable  $R(x)$  is only relevant to the distance between the positions of particles and TE. Therefore, the particle state variables of the two types of devices are unified into the variables of the distance between CF and TE. The compact model is simplified by this assumption and the calculation in circuit simulation is accelerated. Meanwhile, Ohm's law can be applied between the memristor voltage and current

$$i_R = \frac{V_R}{R(x)}. \quad (4)$$

The derivative of  $x$  with respect to time depends on the ion transport rate, i.e., temperature, electric field, and other factors. In this paper, the electric field force, local Joule heat, and interfacial minimum potential energy effect are considered, which are defined as  $f_{\text{drift}}$ ,  $f_{\text{heat}}$ , and  $f_{\text{diffusion}}$ , respectively. The model will represent the drift memristors when  $f_{\text{drift}}$  and  $f_{\text{heat}}$  dominate the movement of particles, while the model will be the diffusion mode when  $f_{\text{drift}}$ ,  $f_{\text{heat}}$ , and  $f_{\text{diffusion}}$  lead.

For the drift memristor, according to [8], the developed resistance model is expressed as

$$f(V, T, x) = f_{\text{drift}}(\text{heat}) \\ = -\mu_0 \cdot \left[ \exp\left(-\frac{qE_{\text{ag}}}{k_B T}\right) \cdot \exp\left(\frac{\gamma d_0 q V_{\text{in}}}{L k_B T}\right) \right. \\ \left. - \exp\left(-\frac{qE_{\text{ar}}}{k_B T}\right) \cdot \exp\left(-\frac{\gamma d_0 q V_{\text{in}}}{L k_B T}\right) \right] \quad (5)$$

$$\frac{dT}{dt} = C_{\text{th}} \cdot \frac{V_{\text{in}}^2}{R_{\text{drift}}} - \kappa(T - T_0) \quad (6)$$

$$R_t = \frac{V_{\text{in}}}{I_0 \exp(-x/x_0) \sinh(V_{\text{in}}/V_0)} \quad (7)$$

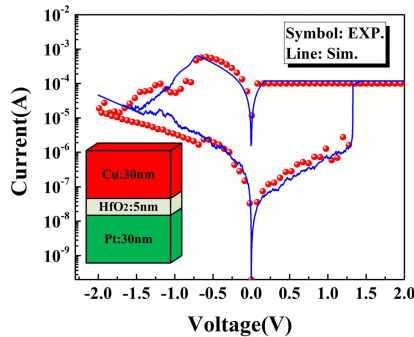


**Fig. 4.** Comparison between the model calculation and experimental data for dc  $I$ - $V$  characteristics of  $\text{HfO}_2$ -based drift memristor.

where the dynamic temperature effect ( $dT/dt$ ) is included [18],  $E_{\text{ag}}$  and  $E_{\text{ar}}$  are the activation energy for vacancy generation and vacancy recombination, respectively [13],  $\mu_0$ ,  $d_0$ ,  $\gamma$ ,  $x_0$ ,  $I_0$ , and  $V_0$  are the dc fitting parameters,  $q$  is the charge,  $k_B$  is Boltzmann's constant,  $L$  is the thickness of resistive layer,  $V_{\text{in}}$  is the voltage between TE and BE of the memristor,  $C_{\text{th}}$  is the heat capacitance,  $\kappa$  is the heat transfer coefficient, and  $T_0$  is the home temperature.

For the diffusion memristor, according to [1] and [20], the interfacial energy for particle diffusion is included, and the model is shown as

$$f(V, T, x) = f_{\text{drift}} + f_{\text{heat}} + f_{\text{diffusion}} \quad (8)$$

$$f_{\text{drift}} = \alpha \frac{V_{\text{in}}}{L} \quad (9)$$

$$f_{\text{heat}} = \sqrt{2\eta k_B T} \quad (10)$$

$$f_{\text{diffusion}} = 2\omega_i \cdot \frac{x - x_c}{R_i^2} \cdot \exp \left[ -\frac{(x - x_c)^2}{R_i^2} \right] + \pi \cdot \frac{\omega_p}{R_p} \cdot \cos \frac{2\pi x}{R_p} \quad (11)$$

$$\frac{dT}{dt} = C_{\text{th}} \cdot \frac{V_{\text{in}}^2}{R_{\text{diffusion}}} - \kappa(T - T_0) \quad (12)$$

$$R_t = R_b \cdot \left[ \exp \left( \frac{x_T - x}{\lambda} \right) - 1 \right] \quad (13)$$

where  $\alpha$  is the electric field fitting factor,  $\eta$  is the particle viscosity coefficient,  $x_c$  is the location of cluster[1], [19],  $x_T$  is the location of TE in the diffusion memristor,  $\omega_i$  is the interfacial energy barrier,  $\omega_p$  is the pinning potential,  $R_i$  and  $R_p$  are location fitting parameters,  $\lambda$  is the effective tunneling length, and  $R_b$  is the resistance state fitting parameter of the diffusion memristor.

### III. DEVICE AND CIRCUIT SIMULATIONS

#### A. Model Verification

To verify the improved model, the dc and ac simulations are carried out in different device modes, and the simulation results are compared with the experimental results. Fig. 4 shows the comparison between the experimental data and model simulation of drift memristor devices with  $\text{HfO}_2$  material as a resistive layer. The model agrees well with the measured data.

The thickness of the resistive material layer has a great influence on the device characteristics [22]. The dc characteristic

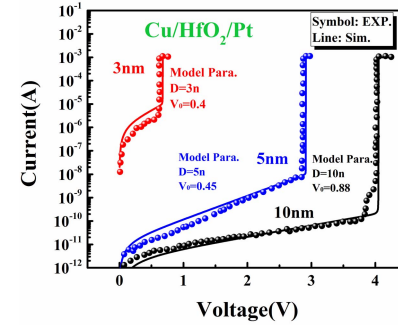


**Fig. 5.** DC characteristic of different thicknesses for  $\text{HfO}_2$  material, compared between the model and experiments.

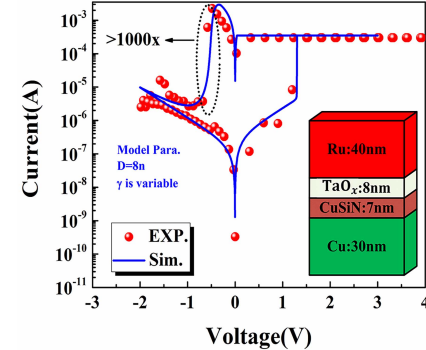


**Fig. 6.** Compared results of another oxide layer material,  $\text{TaO}_2$  resistive layer, and  $\text{CuSiN}$  interface layer of the drift memristor.

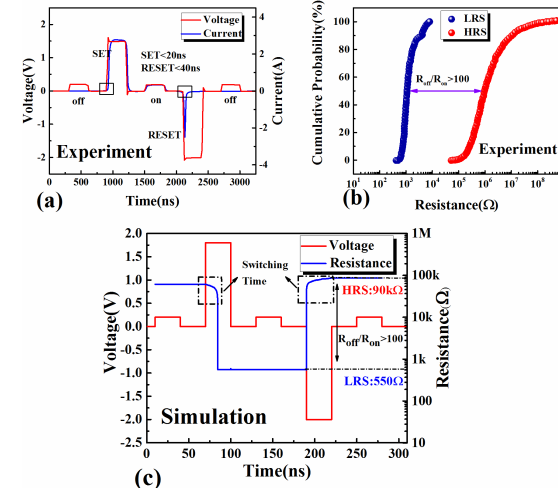


**Fig. 7.** Verification of the drift memristor for transient. (a) Experimental transition characteristics: transition time (both SET and RESET) less than 40 ns. (b) High and low resistance distribution of real device: the  $R_{\text{OFF}}/R_{\text{ON}}$  window is greater than 100. (c) Simulations transition characteristics: transition time (both SET and RESET) less than 40 ns and the  $R_{\text{OFF}}/R_{\text{ON}}$  window is greater than 100.

of the devices with different  $\text{HfO}_2$  thicknesses is shown in Fig. 5. The experimental results can be well reproduced by the model after adjusting the related parameters  $d_0$  and  $V_0$  in (5). The model is also suitable for other oxide layer materials in drift memristors, such as the composite of a  $\text{TaO}_x$  resistive layer and a  $\text{CuSiN}$  interface layer [18], as shown in Fig. 6. The  $I$ - $V$  characteristics of various types of resistive materials can be fitted by the model, after adjusting the fitting parameter  $\gamma$ . In addition, the transient characteristics of the real devices and the model are shown in Fig. 7. The distribution of

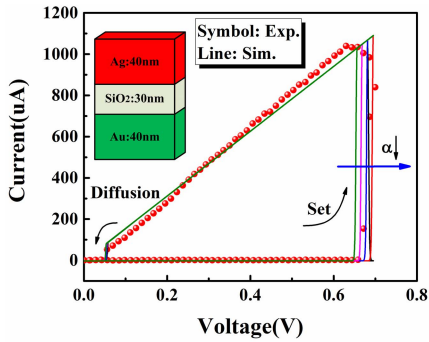


**Fig. 8.** DC characteristic comparison of the  $\text{SiO}_2$ -based diffusion memristor and its model.

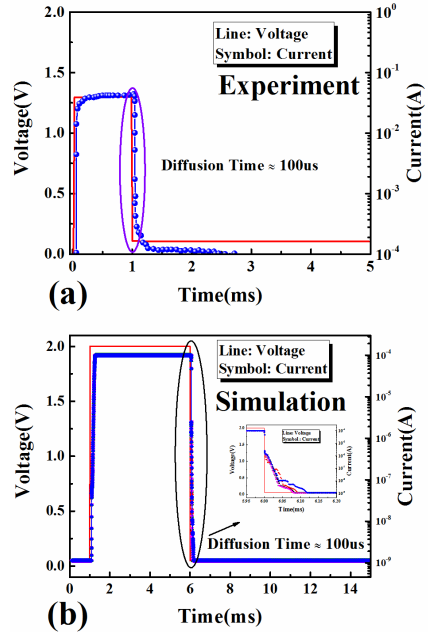


**Fig. 9.** Verification of the diffusion memristor for transient. (a) Experimental transition characteristics: diffusion time is about 100 ns. (b) Simulations transition characteristics: the magnitude of diffusion time is the same as the experimental result.

HRS/LRS and the time of the resistance transition both play an important role in the circuit design [23]. It can be seen from the distributions of the high and low resistance in Fig. 7(c), the  $R_{\text{OFF}}/R_{\text{ON}}$  window is larger than 100, where the resistance in HRS is  $90 \text{ k}\Omega$  and in LRS is  $500 \Omega$ , consistent with the experimental transient simulation results in Fig. 7(b), and the transition time shows the same magnitude, as shown in Fig. 7(a), which is less than 40 ns.

Moreover, this model is most useful in modeling the behavior of the diffusion memristor while the interfacial energy is applied. Fig. 8 displays the  $I$ - $V$  characteristic comparison of the diffusion memristor and its model. In Fig. 9, the model can simulate the transient characteristics of the diffusion memristor with the magnitude of diffusion time matching the experimental result and it can dynamically adjust the parameters between the voltage and the diffusion time. The parameter variation can also be included in the model using the random sequence  $\chi(i)$  in (3) [8]. Considering the parameter variations, the comparison between the model and experimental data is shown in Fig. 10.

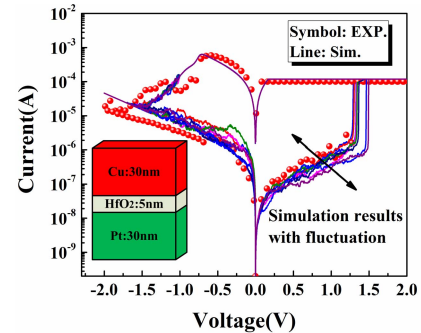


**Fig. 10.** Model verification with parameters fluctuation, for dc  $I$ - $V$  characteristics of  $\text{HfO}_2$ -based drift memristors.

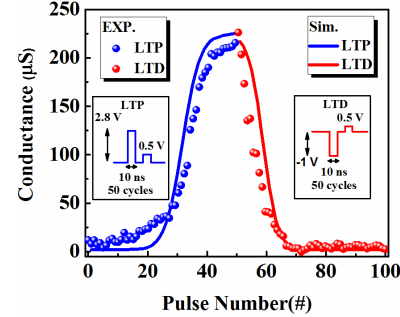


**Fig. 11.** Comparison of experimental data and simulation results of LTP and LTD of  $\text{HfO}_2$ -based drift memristor. Inset: voltage pulse applied in the simulation.

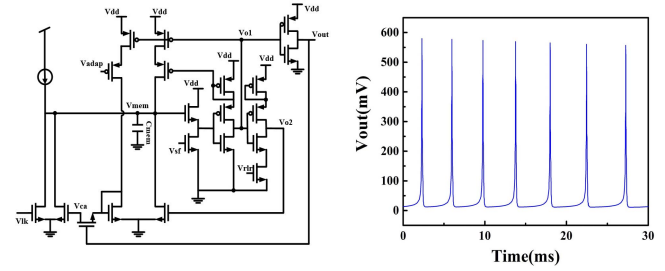


**Fig. 12.** (a) Traditional CMOS IF circuit. (b) CMOS IF circuit simulation results.

Long-term potentiation (LTP) and long-term depression (LTD) [24], [25] are important features of the synaptic device. Fig. 11 shows the drift devices in the process of LTP and LTD under continuous narrow pulse, and the simulation results agree well with the experimental data. The diffusion memristor, however, is difficult to explain the LTP and LTD because of its poor retention.

### B. Circuit Simulation

It is proved that the diffusion memristor can be simulated as the neuromorphic device [1], [20], [26]. Using the developed diffusion memristor Verilog-A model, we can simulate the typical neuromorphic circuits such as integrate-and-fire (IF) [26] and Hodgkin–Huxley (H–H) model circuits [27], [28]. The IF model circuit in Fig. 13 is constructed by diffusion memristors [20]. Response behaviors are consistent with the traditional CMOS circuit shown in Fig. 12, indicating that the IF circuit can be fully implemented using the diffusion memristor device compact model. The pulse frequency of IF circuits is

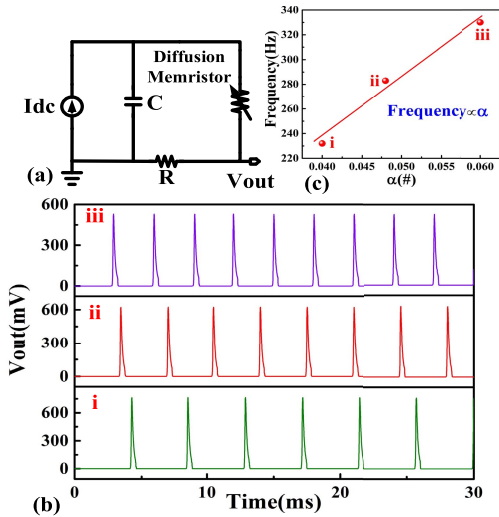


**Fig. 13.** (a) New integrated circuit using the diffusion memristor devices. (b) Simulation results with different  $E$ -field factors. (c) IF circuit frequency is proportional to  $E$ -field factors.

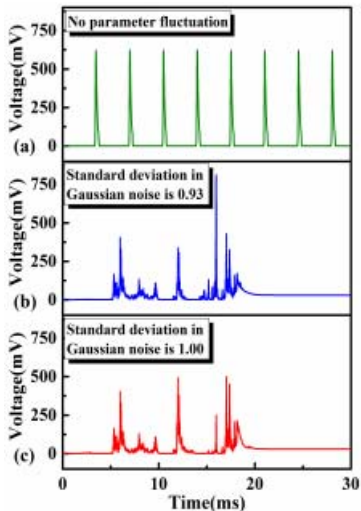


**Fig. 14.** Simulations of IF circuit using the diffusion devices with different parameter fluctuations. (a) Without the Gaussian noise sequence. (b) Standard deviation in Gaussian noise is 0.93. (c) Standard deviation in Gaussian noise is 1.00.

proportional to different electric field forces (the  $E$ -field factors) shown in Fig. 13(b) and (c).

The effect of the switching parameter fluctuation on the circuit performance is shown in Fig. 14. With different parameter fluctuations, the amplitude of the signal consisting of “noise pulse” has different fluctuations. It is indicated that the new integrated circuit using the diffusion memristor devices can reproduce the noise performance of the IF circuits well.

The H–H model circuits can be used to simulate the transmission of neuromorphic signals. Fig. 15(a) shows the H–H model circuit’s structure made by the diffusion memristors. The all-or-nothing and threshold-driven spiking using the compact model of the diffusion memristors for simulation are clearly shown in Fig. 15(b). According to [28], the threshold voltage of the H–H model circuits induces the resistance switching from the HRS to the LRS, corresponding to the SET voltage here, which is very important for the circuit simulation. For the superthreshold region ( $2 \mu\text{A}, 500 \mu\text{s}$ ),

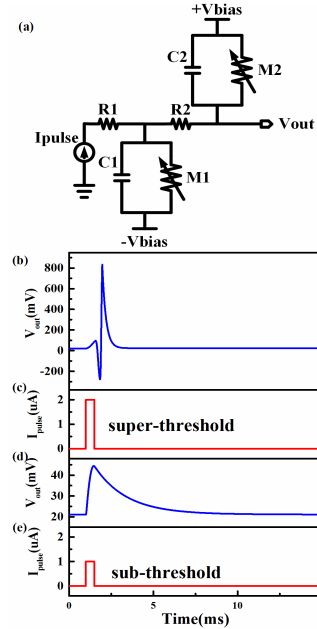


**Fig. 15.** Circuit and simulation results of the H–H model with the diffusion memristor model. (a) M1 and M2 are diffusion memristor devices. (b) and (c) Model simulation results of over threshold. (d) and (e) Model simulation results of subthreshold.

**TABLE I**  
SUMMARY ABOUT THE UNIVERSAL COMPACT MODEL

	Drift memristor	Diffusion memristor
Main feature in neuron	Weight Retention	Threshold Self-restoring
Fluctuation	Enable	Enable
LTD&LTP	Enable	---
IF Circuit	---	Enable
H–H Circuit	---	Enable

Self-restoring: Resistance state switching from HRS to LRS without external voltage.

the circuit will generate a complete action potential, as shown in Fig. 15(b) and (c). For the subthreshold region ( $1 \mu\text{A}, -500 \mu\text{s}$ ), the circuit does not work and will not generate the action potential signal [Fig. 15(d) and (e)]. Here, the drift memristor is unsuitable for the H–H circuit because the drift devices cannot switch from LRS to HRS without the help of applying voltage, and on the contrary, the diffusion memristor can be applied in the H–H circuits.

Finally, Table I gives a summary of the applicability of both drift and diffusion memristors in neuromorphic circuits.

#### IV. CONCLUSION

A compact model applicable for both drift and diffusion memristors is presented, which can compensate the lack of the diffusion memristor model of the neuromorphic device. The model can reproduce the dc and ac characteristics of the device accurately comparable with the measurements of the experiments. The Verilog-A model for SPICE can be used for the neuromorphic circuit design. Moreover, it is found that

the diffusion memristor is more suitable for the neuromorphic circuit. The effect from the device threshold voltage and parameter variations on the circuit performance was discussed.

## REFERENCES

- [1] Z. Wang *et al.*, "Memristors with diffusive dynamics as synaptic emulators for neuromorphic computing," *Nature Mater.*, vol. 16, no. 1, pp. 101–108, Sep. 2016, doi: [10.1038/nmat4756](https://doi.org/10.1038/nmat4756).
- [2] L. O. Chua, "Memristor—the missing circuit element," *IEEE Trans. Circuit Theory*, vol. CT-18, no. 5, pp. 507–519, Sep. 1971, doi: [10.1109/TCT.1971.1083337](https://doi.org/10.1109/TCT.1971.1083337).
- [3] S. H. Jo, T. Chang, I. Ebong, B. B. Bhadviya, P. Mazumder, and W. Lu, "Nanoscale memristor device as synapse in neuromorphic systems," *Nano Lett.*, vol. 10, no. 4, pp. 1297–1301, 2010, doi: [10.1021/nl904092h](https://doi.org/10.1021/nl904092h).
- [4] M. Preziosi, F. Merrikh-Bayat, B. D. Hoskins, G. C. Adam, K. K. Likharev, and D. B. Strukov, "Training and operation of an integrated neuromorphic network based on metal-oxide memristors," *Nature*, vol. 521, pp. 61–64, May 2015, doi: [10.1038/nature14441](https://doi.org/10.1038/nature14441).
- [5] R. Waser and M. Aono, "Nanoionics-based resistive switching memories," *Nature Mater.*, vol. 6, no. 11, pp. 833–840, Nov. 2007, doi: [10.1038/nmat2023](https://doi.org/10.1038/nmat2023).
- [6] Y. V. Pershin and M. Di Ventra, "Experimental demonstration of associative memory with memristive neural networks," *Neural Netw.*, vol. 23, no. 7, pp. 881–886, 2010, doi: [10.1016/j.neunet.2010.05.001](https://doi.org/10.1016/j.neunet.2010.05.001).
- [7] Y. Zhao *et al.*, "A physics-based compact model for material- and operation-oriented switching behaviors of CBRAM," in *IEDM Tech. Dig.*, Dec. 2017, pp. 7.6.1–7.6.4, doi: [10.1109/IEDM.2016.7838370](https://doi.org/10.1109/IEDM.2016.7838370).
- [8] Z. Jiang, S. Yu, Y. Wu, J. H. Engel, X. Guan, and H.-S. P. Wong, "Verilog—A compact model for oxide-based resistive random access memory (RRAM)," in *Proc. IEEE Int. Conf. Simulation Semiconductor Processes Devices*, Sep. 2014, pp. 41–44, doi: [10.1109/SISPAD.2014.6931558](https://doi.org/10.1109/SISPAD.2014.6931558).
- [9] J. Kang *et al.*, "Oxide-based RRAM: Requirements and challenges of modeling and simulation," in *IEDM Tech. Dig.*, Dec. 2015, pp. 5.4.1–5.4.4, doi: [10.1109/IEDM.2015.7409634](https://doi.org/10.1109/IEDM.2015.7409634).
- [10] Z. Jiang *et al.*, "A compact model for metal-oxide resistive random access memory with experiment verification," *IEEE Trans. Electron Devices*, vol. 63, no. 5, pp. 1884–1892, May 2016, doi: [10.1109/TED.2016.2545412](https://doi.org/10.1109/TED.2016.2545412).
- [11] H. Li *et al.*, "Variation-aware, reliability-emphasized design and optimization of RRAM using SPICE model," in *Proc. Design, Automat. Test Eur. Conf. Exhib. (DATE)*, Mar. 2015, pp. 1425–1430, doi: [10.7873/DATE.2015.0362](https://doi.org/10.7873/DATE.2015.0362).
- [12] Z. Jiang *et al.*, "Microsecond transient thermal behavior of HfO<sub>x</sub>-based resistive random access memory using a micro thermal stage (MTS)," in *IEDM Tech. Dig.*, Dec. 2017, pp. 21.3.1–21.3.4, doi: [10.1109/IEDM.2016.7838465](https://doi.org/10.1109/IEDM.2016.7838465).
- [13] P.-Y. Chen and S. Yu, "Compact modeling of RRAM devices and its applications in 1T1R and 1S1R array design," *IEEE Trans. Electron Devices*, vol. 62, no. 12, pp. 4022–4028, Dec. 2015, doi: [10.1109/TED.2014.2492421](https://doi.org/10.1109/TED.2014.2492421).
- [14] D. Biolek, Z. Kolka, V. Biolkova, and Z. Biolek, "Memristor models for SPICE simulation of extremely large memristive networks," in *Proc. IEEE Int. Symp. Circuits Syst.*, May 2016, pp. 389–392, doi: [10.1109/ISCAS.2016.7527252](https://doi.org/10.1109/ISCAS.2016.7527252).
- [15] T. Chang, S.-H. Jo, K.-H. Kim, P. Sheridan, S. Gaba, and W. Lu, "Synaptic behaviors and modeling of a metal oxide memristive device," *Appl. Phys. A*, vol. 102, no. 4, pp. 857–863, 2011, doi: [10.1007/s00339-011-6296-1](https://doi.org/10.1007/s00339-011-6296-1).
- [16] K.-H. Hsu, W.-W. Ding, and M.-H. Chiang, "A compact SPICE model for bipolar resistive switching memory," in *Proc. IEEE Int. Conf. Electron Devices Solid-State Circuits*, Jun. 2013, pp. 1–2, doi: [10.1109/EDSSC.2013.6628127](https://doi.org/10.1109/EDSSC.2013.6628127).
- [17] F. García-Redondo, R. P. Gowers, A. Crespo-Yepes, M. López-Vallejo, and L. Jiang, "SPICE compact modeling of bipolar/unipolar memristor switching governed by electrical thresholds," *IEEE Trans. Circuits Syst. I, Reg. Papers*, vol. 63, no. 8, pp. 1255–1264, Aug. 2016, doi: [10.1109/TCSI.2016.2564703](https://doi.org/10.1109/TCSI.2016.2564703).
- [18] F. O. Hatem, T. N. Kumar, and H. A. F. Almurib, "A SPICE model of the Ta<sub>2</sub>O<sub>5</sub>/TaO<sub>x</sub>Bi-Layered RRAM," *IEEE Trans. Circuits Syst. I, Reg. Papers*, vol. 63, no. 9, pp. 1487–1498, Sep. 2016, doi: [10.1109/TCSI.2016.2579503](https://doi.org/10.1109/TCSI.2016.2579503).
- [19] R. Midya *et al.*, "Anatomy of Ag/hafnia-based selectors with 1010 nonlinearity," *Adv. Mater.*, vol. 29, no. 12, p. 1604457, Jan. 2017, doi: [10.1002/adma.2016.04457](https://doi.org/10.1002/adma.2016.04457).
- [20] Z. Wang *et al.*, "Fully memristive neural networks for pattern classification with unsupervised learning," *Nature Electron.*, vol. 1, pp. 137–145, Feb. 2018, doi: [10.1038/s41928-018-0023-2](https://doi.org/10.1038/s41928-018-0023-2).
- [21] D. B. Strukov, G. S. Snider, D. R. Stewart, and R. S. Williams, "The missing memristor found," *Nature*, vol. 453, pp. 80–83, May 2008, doi: [10.1038/nature06932](https://doi.org/10.1038/nature06932).
- [22] M. Wang *et al.*, "Study of one dimension thickness scaling on Cu/HfO<sub>x</sub>/Pt based RRAM device performance," in *Proc. 4th IEEE Int. Memory Workshop (IMW)*, May 2012, pp. 1–3, doi: [10.1109/IMW.2012.6213627](https://doi.org/10.1109/IMW.2012.6213627).
- [23] S. Liu *et al.*, "Highly improved resistive switching performances of the self-doped Pt/HfO<sub>2</sub>:Cu/Cu devices by atomic layer deposition," *Sci. China Phys., Mech. Astron.*, vol. 59, p. 127311, Dec. 2016, doi: [10.1007/s11433-016-0389-9](https://doi.org/10.1007/s11433-016-0389-9).
- [24] X. Zhang *et al.*, "Emulating short-term and long-term plasticity of biosynapse based on Cu/A-Si/Pt memristor," *IEEE Electron Device Lett.*, vol. 38, no. 9, pp. 1208–1211, Sep. 2017, doi: [10.1109/LED.2017.2722463](https://doi.org/10.1109/LED.2017.2722463).
- [25] X. Yan *et al.*, "Memristor with Ag-cluster-doped TiO<sub>2</sub> films as artificial synapse for neuroinspired computing," *Adv. Funct. Mater.*, vol. 28, no. 1, p. 1705320, 2017, doi: [10.1002/adfm.201705320](https://doi.org/10.1002/adfm.201705320).
- [26] X. Zhang *et al.*, "An artificial neuron based on a threshold switching memristor," *IEEE Electron Device Lett.*, vol. 39, no. 2, pp. 308–311, Feb. 2018, doi: [10.1109/led.2017.2782752](https://doi.org/10.1109/led.2017.2782752).
- [27] R. Appali, S. Petersen, and U. van Rienen, "A comparison of Hodgkin-Huxley and soliton neural theories," *Adv. Radio Sci.*, vol. 8, no. 6, pp. 75–79, 2010, doi: [10.5194/ars-8-75-2010](https://doi.org/10.5194/ars-8-75-2010).
- [28] M. D. Pickett, G. Medeiros-Ribeiro, and R. S. Williams, "A scalable neuristor built with Mott memristors," *Nature Mater.*, vol. 12, pp. 114–117, Dec. 2012, doi: [10.1038/nmat3510](https://doi.org/10.1038/nmat3510).



**Ying Zhao** is currently pursuing the master's degree with the University of Electronic Science and Technology of China, Chengdu, China.

She is currently involved in the compact model of MOSFET and machine learning model for devices.



**Cong Fang** is currently pursuing the master's degree with Beijing Jiaotong University, Beijing, China.

His current research interests include analog integrated circuit design and memory SPICE model design.



**Xumeng Zhang** is currently pursuing the Ph.D. degree with the Institute of Microelectronics of Chinese Academy of Sciences, Beijing, China.

His current research interests include memristor, bioinspired computing, and performance optimization for memory device.



**Xiaoxin Xu** is with the Institute of Microelectronics of Chinese Academy of Sciences, Beijing, China. She is currently involved in the reliability optimization and integration of the resistive non-volatile memory and energy-efficient electronic devices. She has co-authored over 50 technical papers.



**Hangbing Lv** is a full Professor with the Key Laboratory of Microelectronics Devices and Integrated Technology, Institute of Microelectronics of Chinese Academy of Sciences, Beijing, China. His current research interests include emerging nonvolatile memory device and application, 3-D integration, and neuromorphic computing.



**Tiancheng Gong** is currently pursuing the Ph.D. degree with the Institute of Microelectronics of Chinese Academy of Sciences, Beijing, China.

His current research interests include reliability analysis and 3-D integration techniques of RRAM.



**Qiang Li** (S'04–M'07–SM'13) is currently a Full Professor with the University of Electronic Science and Technology of China, Chengdu, China, where he is the Head of the Institute of Integrated Circuits and Systems. His current research interests include low-voltage and low-power analog/RF circuits, data converters, and mixed-mode circuits for biomedical and sensor interfaces.



**Qing Luo** is currently an Assistant Professor with the Key Laboratory of Microelectronics Devices and Integrated Technology, Institute of Microelectronics of Chinese Academy of Sciences, Beijing, China. His current research interests include 3-D integration techniques of RRAM.



**Feng Zhang** is currently a Full Professor with the Institute of Microelectronics of Chinese Academy of Sciences, Beijing, China. His current research interests include low-power low-jitter clock synthesis/recovery circuits (phase-locked loop), low-power high-speed I/O links, and low-power high-speed memory design.



**Chengying Chen** received the Ph.D. degree from the University of Chinese Academy of Sciences, Beijing, China, in 2016.

He is currently an Associate Professor with the School of Microelectronics, Xiamen University of Technology, Xiamen, China. His current research interests include low-power analog integrated circuit and memory design.



**Ling Li** is currently a Professor with the Institute of Microelectronics of Chinese Academy of Sciences, Beijing, China. His current research interests include charge transport in disordered material, device modeling, and circuit design issues.



**Qi Liu** is currently a Professor with the Institute of Microelectronics of Chinese Academy of Sciences, Beijing, China.

His current research interests include fabrication, characterization, and mechanism of the emerging memristor devices for nonvolatile memory, logic circuit, and neuromorphic computing applications.



**Ming Liu** (M'08–SM'10–F'18) is currently the Director of the Key Laboratory of Microelectronics Devices and Integrated Technology, Institute of Microelectronics of Chinese Academy of Sciences, Beijing, China, where he is also a Professor. Her current research interests include semiconductor materials, integrated-circuit processing, nanofabrication, nanoelectronics, molecular electronics, and flash memory.